

Multi-Layered Automultiscopic Displays

Nicola Ranieri¹ Simon Heinze² Quinn Smithwick³ Daniel Reetz³ Lanny S. Smoot³ Wojciech Matusik⁴ Markus Gross^{1,2}

¹ETH Zurich ²Disney Research Zurich ³Disney Research Glendale ⁴MIT CSAIL

Abstract

Our hybrid display model combines multiple automultiscopic elements volumetrically to support horizontal and vertical parallax at a larger depth of field and better accommodation cues compared to single layer elements. In this paper, we introduce a framework to analyze the bandwidth of such display devices. Based on this analysis, we show that multiple layers can achieve a wider depth of field using less bandwidth compared to single layer displays. We present a simple algorithm to distribute an input light field to multiple layers, and devise an efficient ray tracing algorithm for synthetic scenes. We demonstrate the effectiveness of our approach by both software simulation and two corresponding hardware prototypes.

Categories and Subject Descriptors (according to ACM CCS): I.3.1 [Computer Graphics]: Hardware Architecture—Three-dimensional displays;

1. Introduction

Displays that provide the illusion of three dimensions have become increasingly popular. Although the majority of current 3D displays rely on the use of special glasses, it is generally agreed that multi-view autostereoscopic displays – unencumbered by glasses and providing a large viewing range – offer significant advantages. These displays make steady technological progress in terms of resolution and perceived quality. The illusion of three dimensions is created by physically separating viewing rays originating from a display surface. However, extremely high resolution is usually required in order to satisfy the depth range of typical 3D scenes and to avoid aliasing artifacts. This problem is even more pronounced for displays that support both horizontal and vertical parallax.

In this paper we introduce multi-layered automultiscopic displays for 4D light fields. Our hybrid display model volumetrically combines multiple automultiscopic layers and supports horizontal and vertical parallax, and it supports better accommodation cues than single layer elements. Furthermore, multi-layered displays are able to use the available display bandwidth more efficiently. The combined bandwidth of n layers only requires $\frac{1}{n}$ of the total ray count of a single layer display to show the same diffuse scene content with approximated occlusions. An efficient algorithm can be used to decompose an input light field for such multi-layered configurations. For synthetic scenes, we propose a very simple ex-

tension to existing ray tracers that supports spatial and angular anti-aliasing using super-sampling. In order to show the effectiveness of our approach, we simulate different configurations of multi-layered automultiscopic displays. We also present two physical prototypes implementing our display model. The first prototype uses two parallax-based color displays that are superimposed onto the same optical path using a beam-splitter. The second prototype uses a varifocal mirror to optically replicate one integral imaging-based monochrome display onto multiple depth planes using temporal multiplexing, supporting up to 24 layers of depth.

2. Related Work

Parallax barriers. Parallax barrier displays employ modulated blocking patterns to provide different viewing rays for different viewing angles. This concept was introduced by Frederic Ives using static parallax stereograms [Ive03]. Enabled by the advent of LCD technology, Isono et al. [IYS93] proposed dynamic parallax barrier displays for autostereoscopic content. Jacobs et al. [JMW*03] later developed a parallax barrier display able to switch between a high-resolution 2D display and a lower resolution autostereoscopic display. Kim et al. [KKK*07] then extended this concept to time-multiplexed parallax barriers to improve the perceived spatial sampling resolution for automultiscopic displays. Instead of increasing the sampling resolution, Perlin et al. [PPK00] and Peterka et al. [PKS*08] tracked the viewer's

location to adapt stereoscopic content. More recently, Lanman et al. [LHKR10] introduced content-adaptive parallax displays that dynamically optimize the barriers based on factored light field data.

Integral imaging. In 1908, Lippmann [Lip08] published his seminal paper on integral imaging. He proposed using small lenticular lenses to provide different viewing rays for different angles, similar to parallax barriers but at higher brightness. Many improvements to Lippmann’s basic lenticular array idea have been proposed, and a thorough overview of recent advances is given in [KHL10]. For instance, apparent resolution can be enhanced by using slanted lenticular sheets arranged with respect to LCD subpixels [Ber99] or by spatio-temporal multiplexing [JJ02]. Fuchs et al. [FRSL08] present a display system based on regular lenticulars which, in contrast to all prior work, relies additionally on the incident illumination angles to support ambient lighting-dependent effects. Kao et al. [KHY*09] present a display that changes the focal length of all lenses simultaneously in order to adapt to the viewer’s distance.

Volumetric displays. Instead of multiplexing light rays for different directions, volumetric displays create a volume of individually controlled light sources. Tamura and Tanaka [TT82] employed beam-splitters to superimpose multiple 2D displays onto a single optical path. In contrast to a multi-layer approach, Buzak [Buz85] developed a field-sequential display using a set of electrically switchable bi-state mirrors that reflect or transmit the light dynamically to change the apparent distance to the display plane. Leung et al. [LIE98] proposed using a light panel followed by a stack of light absorbing LCD panels to achieve a depth volume, similar to the multi-layered displays of PureDepth Inc. [BCP*08]. Gold and Freeman [GF98] developed a field-sequential display system using a projector in conjunction with set of bi-state optical shutters able to switch between transparent and translucent state. The DepthCube system by Sullivan [Sul04] extended this concept by employing a high-speed projector and 20 shutter screens. Suyama et al. [STUS00, SSH*04] built systems that approximate depth by interpolating between two different depth planes, and more recently, Uehira [Ueh07] studied the ability of the human visual system to fuse two different autostereoscopic displays positioned at different depth planes. Traub [Tra67] presented a volumetric display based on a vibrating varifocal mirror to extrude a display surface into space, thus creating multiple display layers. For a more comprehensive overview of previous volumetric displays, we refer to Favalora’s survey article [Fav05]. Unfortunately, all of these volumetric displays cannot represent occlusion or view-dependent effects.

There are a few notable volumetric displays capable of providing occlusion. The static multi-layer display presented by Holroyd et al. [HBLM11] uses display layers printed on transparencies embedded between acrylic plates. The closely

related displays by Cossairt et al. [CNH*07] and Jones et al. [JMY*07] effectively display a 360 degree light field of a scene within the working volume. Although called volumetric, these displays are, in fact, quite similar to parallax barriers. Instead of using blocking patterns to provide different viewing rays for different viewing angles, they employ time multiplexing with a high-speed projector and a rotating vertical anisotropic mirror to attain the same effect. Finally, the display system by Akeley et al. [AWGB04] supports true autostereoscopic viewing with occlusion and better accommodation cues, but for one fixed viewpoint only.

Multi-layer displays. Gotoda [Got10] presented a novel display device by stacking multiple LCD panels on the top of a uniform light source. His display uses volumetric attenuation to display autostereoscopic content. Wetzstein et al. [WLHR11] extended the idea and employed tomographic reconstruction techniques to create this light-attenuating volume to display 4D light field images. Their thorough bandwidth analysis showed that the available bandwidth can be used more efficiently compared to single-layer automultiscopic displays, at a moderate field of view. Lanman et al. [LWH*11] adapt this technique by reformulating the problem to switching LCDs instead of modulating layers, and show a real-time prototype using multiple stacked LCD screens. Most recently, Wetzstein et al. [WLHR12] extended this concept to multiple stacked LCD screens combined with temporal multiplexing and directional backlighting to enhance the field of view and display quality of attenuation-based multi-layer displays.

Multi-layered automultiscopic displays. Similar to previous work, our display prototype also consist of multiple layers; however, instead of attenuating light, our display additively combines multiple parallax based displays to increase the effective bandwidth usage. In contrast to previous volumetric displays based on multiple layers, our display is a hybrid volumetric display with view dependent pixels, and our display is therefore able to support with occlusion in addition to relatively wide viewing angles and parallax.

3. Multi-Layered Automultiscopic Displays

In this paper we introduce multi-layered automultiscopic displays, a hybrid display model that combines the benefits of volumetric and parallax-based displays. The idea is very simple: multiple translucent display layers at different depths are combined onto the same optical path. In contrast to previous volumetric displays, each of the layers is comprised of an automultiscopic layer to emit true view dependent rays. Our display model is therefore very similar to volumetric displays, however, capable of view-dependent occlusion.

Figure 1 illustrates this concept for a dual-layer configuration. Each automultiscopic layer consists of two planes. Rays are generated on the *emissive back plane* with angular

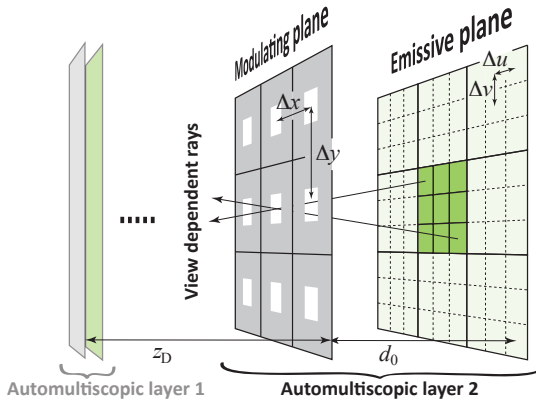


Figure 1: Multi-layered automultiscopic display for 4D light fields. Each layer consists of an automultiscopic display, e.g. using parallax barriers (shown here) or lenslet arrays. The layers are multiplexed on the same optical path. Rays are generated on an emissive plane, and spatially separated into view-dependent rays on the modulating plane.

sampling ($\Delta u, \Delta v$). The emissive pixels are spatially separated into view-dependent rays, using pinholes on the *modulating front plane*, with spatial sampling ($\Delta x, \Delta y$). The emissive and modulating plane of each layer are separated by a distance d_0 , the layers themselves are positioned at a distance z_D apart. The individual automultiscopic layers are then superimposed onto the same optical path, at different depths. Note that we assume that our layers cannot support true occlusion, i.e., a display layer cannot block light from any back layer.

3.1. Light Field Distribution

For a given display configuration, the input light field $\ell_{IN}(x, y, u, v)$ needs to be distributed to the individual display layers $Layer_i$. In principle, our distribution algorithm is very simple. For each output light field ℓ_{OUT_i} , assign each ray from ℓ_{IN} to the display layer $Layer_i$ closest to the ray origin.

Due to the nature of our display, front layers cannot block incoming light from the back layers. Such occlusions can implicitly be handled by the light field distribution: occlusions are represented as rays with zero luminance in the respective output light fields ℓ_{OUT_i} . Intuitively, these occlusions correspond to a shadow that is cast by an occluder on all the following display planes. Note, that rays generated outside the depth range of the layers (including object shadows) can lead to aliasing. In order to avoid such aliasing, the output light fields need to be filtered accordingly, e.g. using a method similar to [ZMDP06]. Algorithm 1 summarizes the light field distribution.

3.2. Ray Tracing Algorithm

Algorithm 1 assumes known depth information for the input light field. For synthetic scenes, this information is already given, and the algorithm can be reformulated as simple modification to any given ray tracing framework. For each layer, the respective depth range is determined. Then, ray tracing is performed within this depth range only. To achieve anti-aliasing comparable to [ZMDP06], we employ spatio-angular multi-sampling: instead of casting one ray only, we stochastically sample the original (x, y, u, v) sampling locations. Algorithm 2 summarizes our extension, note that the depth range of the outermost layers is extended to $\pm\infty$, in order to capture the whole scene.

4. Bandwidth Analysis

In this section we will evaluate the effective bandwidth usage of multi-layered automultiscopic displays. We will start by introducing the bandwidth of a single layer, and will show that much of the available display bandwidth for 4D light fields is unused. We will then show that multiple layers can represent the same frequency content using less overall bandwidth.

Without loss of generality, we will assume a display with uniform spatial sampling $\Delta x = \Delta y$ and uniform angular sampling $\Delta u = \Delta v$ as well as unit spacing $d_0 = 1$ between the (x, y) and (u, v) planes for this derivation.

4.1. Bandwidth of Single Layer

The bandwidth of an automultiscopic display is defined as the range of all possible frequencies that can be represented by the display. As noted by Zwicker et al. [ZMDP06], the maximum spatial and angular frequencies are delimited by $\frac{\pi}{\Delta x}$ and $\frac{\pi}{\Delta u}$. The bandwidth of a display is then defined as

$$H(\omega_x, \omega_y, \omega_u, \omega_v) = \begin{cases} 1, & \text{for } |\omega_{x,y}| \leq \frac{\pi}{\Delta x}, |\omega_{u,v}| \leq \frac{\pi}{\Delta u}, \\ 0, & \text{otherwise.} \end{cases}$$

The bandwidth corresponds to a 4D hyperbox with volume $(2\pi/\Delta x)^2 \cdot (2\pi/\Delta u)^2$, see Figure 2 for an illustration using a 2D cut. As also noted by Zwicker et al. [ZMDP06], much of the available bandwidth will be unused.

According to [CTCS00, LD10], the light field ℓ of a Lambertian plane parallel to the display plane will only exhibit frequency entries on a 2D plane. Therefore, the

Algorithm 1: Light field distribution overview

```

for all rays of input light field  $\ell_{IN}$ 
    Find closest display  $Layer_i$  to ray origin
    Assign ray to output light field  $\ell_{OUT_i}$ 
for all  $Layer_i$ 
     $\ell_{OUT_i} = \text{prefilter}(\ell_{OUT_i})$ 

```

Algorithm 2: Light field ray tracing overview

```

Determine depth ranges of all layers
for each Layeri
  for each sample s emitted from display:
    Generate n rays sampled around (xs, ys, us, vs)
    Intersect rays with scene
    Assign zero luminance if intersection is not in range
    Filter rays

```

light field spectrum $\hat{\ell}$ will contain non-zero entries only on $\hat{\ell}(\omega_x, \omega_y, z\omega_x, z\omega_y)$, where z is the distance of the plane to display. As a consequence, only frequency content lying within a 3D wedge in 4D space can be displayed without aliasing at full spatial resolution. This implies that only a very small subset of the total bandwidth can effectively be used. Furthermore, the bandwidth box delimits the maximum depths that can be displayed without aliasing to $z_{\max} = \pm(\Delta x/\Delta u)$. More specifically, the maximum displayable spatial frequency $\tilde{\omega}_x$ for a plane at distance z can be described as

$$\tilde{\omega}_x(z) = \pm \min\left(\frac{\pi/\Delta u}{z}, \frac{\pi}{\Delta x}\right). \quad (1)$$

The maximum frequency $\tilde{\omega}_y$ follows directly. See Figure 2 for an illustration.

4.2. Bandwidth of Multiple Layers

In the following we will assume layer independence: more specifically, we will assume that each layer can block light incoming light from any back layer. We will first show the bandwidth usage of two automultiscopic layers. Assume that each layer has a quarter of the overall angular sampling $\Delta u' = 2\Delta u$ and $\Delta v' = 2\Delta v$ of a single layer display, and the spatial sampling remains constant. Therefore, the maximum depth that can be displayed without aliasing on a single layer reduces to $z'_{\max} = \pm\Delta x/(2\Delta u) = z_{\max}/2$. In order to cover the same depth range compared to the single layer display, the two layers need to be positioned at $\pm z'_{\max}$ respectively.

The bandwidth of these two layers is smaller than the bandwidth of the single layer display, although it is able to represent the same content within z_{\max} . More specifically, the angular sampling is reduced by $\frac{1}{2}$ in both u and v direction for both display layers. Therefore, the bandwidth of the system reduces to $2 \cdot (2\pi/\Delta x)^2 \cdot (\pi/\Delta u)^2 = \frac{1}{2} \cdot (2\pi/\Delta x)^2 \cdot (2\pi/\Delta u)^2$. As a consequence, two layers can display the same diffuse scene content compared to a single layer, but using only half the number of rays.

By the same geometric construction, the overall bandwidth and ray count for n display layers reduces to $\frac{1}{n}$ compared to a single layer configuration. The maximum depth z_{\max} that can be displayed at full spatial resolution remains identical to the single layer configuration. The maximum

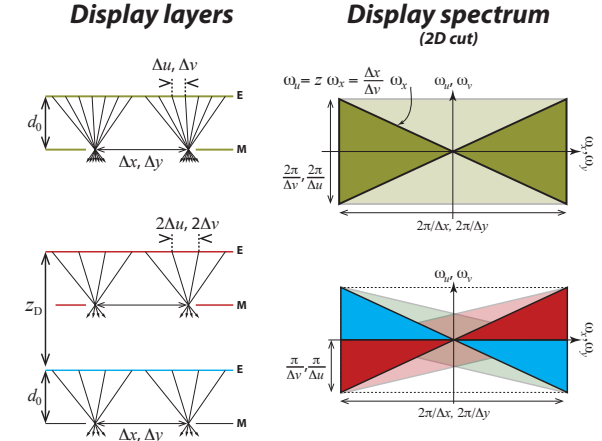


Figure 2: Bandwidth analysis for multi-layered automultiscopic displays, illustrated as a 2D cut through the 4D light field. A single layer display is illustrated in the top row, a dual layer configuration is illustrated in the bottom row. While both configurations share the same spatial resolution, each layer in the dual configuration only requires $\frac{1}{4}$ angular resolution for horizontal and vertical parallax. The solid wedges delimit the frequencies that can be displayed without aliasing at full spatial resolution. The (translucent) rectangular boxes show the overall displayable spatial and angular frequencies for each layer. Both displays exhibit the same depth of field for frequencies at full spatial resolution.

displayable spatial frequency at a distance z from one individual layer $\tilde{\omega}_x^{(l)}$ (positioned at z_l) reduces to $\tilde{\omega}_x^{(l)}(z) = \pm \min\left(\frac{\pi/(n\Delta u)}{z - z_l}, \frac{\pi}{\Delta x}\right)$. Each layer therefore has its own range of displayable frequencies. All layers are additively superimposed, and therefore the individual layers do not influence each other. Due to the overlap of the bandwidth boxes, however, some of frequencies can be displayed on both layers and therefore do not add additional information, see Figure 2. The maximum displayable frequencies of the combined depth of fields can then be described by using the outer layer:

$$\tilde{\omega}_x^{(n)}(z) = \pm \min\left(\frac{\pi/(n\Delta u)}{z - \frac{n-1}{n}z_{\max}}, \frac{\pi}{\Delta x}\right),$$

As long as the light field content is within $\pm z_{\max}$, our multiple layer approach can display the same light field content for diffuse scenes. Outside this depth of field, the possible frequencies are reduced compared to the single layer configuration.

Note, that in the limit ($n \rightarrow \infty$), each layer would only emit one angular sample, and the multi-layered automultiscopic display would resemble to a volumetric display. In this limit case, view dependent effects cannot be supported. Furthermore, our prototypes do not support the blocking of

incoming light. In order to implicitly support occlusions for purely additive layers, occlusions need to be represented as black objects which can lead to aliasing. See Section 7 for more discussion.

If the frequency spectrum is much sparser, the overall bandwidth could be optimized even further for a given scene. For example, a scene could be comprised of a foreground object and a background object separated by a large distance. Then, the display layers could be separated by the same distance in order to optimally use the respective bandwidths. If the scene or the depth separation changes, however, the displays would have to be reconfigured.

5. Software Framework

We implemented our light field distribution algorithm for ray tracing within Optix [PBD^{*}10], a framework for general purpose ray tracing on the GPU. Our implementation performs ray tracing for all layers in parallel, and all rays are generated according to the ray sampling of the layers. Anti-aliasing is achieved by stochastic super-sampling around the original sampling locations, and all samples are interpolated using a box filter. Our ray tracer supports only basic ray-casting only but it could easily be extended for more realistic image generation.

Layer borders. The layer distribution can introduce high frequencies, especially when continuous surfaces are separated by two layers. In order to avoid noisy artifacts, a high number of multi-samples would be necessary. We mitigate these issue using a different strategy. Instead of using binary cuts, our implementation employs ‘fuzzy’ layer borders: we slightly overlap neighboring depth of fields, and we linearly weight the corresponding samples that fall within the overlapping region, with respect to the actual layer borders. This strategy greatly reduces these artifacts without the need for very high sampling densities.

Optimized field of view. Using regular sampling, many rays will fall outside the field of view for close viewing positions. In order to increase the effective ray utilization for a given viewing position, the emitted view rays can be sheared along the angular direction $u' = u + sx$ and $v' = v + sy'$, where s is dependent on the display parameters and viewing distance. In our implementation, we round the sheared rays to the nearest sampling location determined by the pixel grid.

Display simulation. The simulated results have been generated using a custom ray tracer implemented within the Optix framework. Each display layer is represented by two planes. The emitting plane is assigned a luminance texture corresponding to the generated pattern from the light field distribution. The modulating plane is assigned a transmission texture corresponding to the spatial sampling. For the simulation, we apply super-sampling of the viewing rays to approximate cross-talk.

6. Hardware Setups

We evaluate the effectiveness of our algorithm using two hardware prototypes. The first prototype uses two automultiscopic layers superimposed onto the same optical path using a beam-splitter with high resolution, while the second prototype allows us to demonstrate our technique with up to 24 depth planes, but at lower resolution.

6.1. Beam-Splitter Prototype

The setup of the first prototype consists of two automultiscopic layers which are combined onto the same optical path using a beam-splitter, as illustrated in Figure 3. Our custom automultiscopic layers are constructed using two LCD layers stacked on top of each other. The back emissive layer is comprised of a regular LCD display with backlight. The front modulating layer consists of a disassembled and modified LCD panel from a regular LCD display. The diffusing front polarizer and the back polarizer have been removed and replaced with non-diffusing and matching polarizers, rotated by 90 degrees. In order to reduce Moire patterns, an additional diffuser with a small point spread function of approximately one pixel is placed in front of the back LCD. Both LCDs are then stacked on top of each other and physically separated using a layer of acrylic glass. The assembly of one individual layer is very similar to [LHKR10], with the following differences. In their setup, the diffuser exhibits a much larger point spread function, effectively reducing their available display resolution. Furthermore, their modulating LCD features only a front polarizer but no back polarizer. Unfortunately, the diffuser to reduce the Moire pattern destroys much of the polarization from the emissive layer, and using a front polarizer only would not result in sufficient contrast. The LCD panels have been taken from a Acer HN274H display (27", 1920x1080, 120Hz). The panels are driven from a dual-head NVIDIA GTX 580 graphics card.

In order to increase the perceived spatial resolution, we employ time-multiplexing of the parallax barriers similar to Kim et al. [KKK^{*}07]. Synchronization for one automultiscopic layer is performed implicitly by the graphics board. Synchronization between the two automultiscopic layers would require higher end graphics boards, and thus displaying dynamic scenes is not possible with the current prototype. The alignment of the stacked LCDs as well as the automultiscopic layers is currently performed using careful manual adjustment, and could be improved using more advanced assembly setups and by using automated calibration techniques.

6.2. Varifocal Multi-Plane Display

For the second verification of our algorithm we use a setup similar to a recently proposed volumetric display [SSR12]. In its original form, a 60Hz display is used in conjunction with a high-speed DLP projector used as back-light.

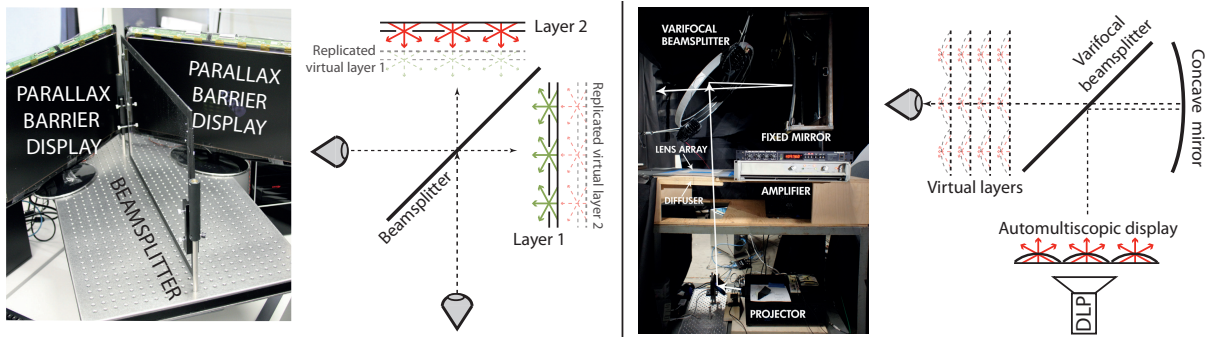


Figure 3: We demonstrate our approach using two different hardware prototypes. The first hardware implementation uses a beam splitter to superimpose two custom-built parallax barrier color displays. The second hardware implementation uses a varifocal beam splitter setup: the central beam splitter is vibrated to virtually position a lenticular-based automultiscopic monochrome display onto many depth planes. Both displays support horizontal and vertical parallax, wide viewing angles and better accommodation cues as single layer displays.

The depth extrusion is achieved using a large vibrating beam-splitter, which is comprised of a metallized Mylar polyester film membrane stretched over a circular hoop. Three equidistant transducers are mounted to the edge of the hoop in order to vibrate the beam-splitter axially. The beam-splitter surface tension is tuned to vibrate at an eigen frequency of 30Hz with a high Q-factor, and as such, its surface becomes alternatively convex and concave. The display surface is relayed by the vibrating beam-splitter towards a fixed concave mirror. The returning light passes through the beamsplitter and forms a real 2.5D stack of 2D images in front of the apparatus. In its current setup, the system is able to create a layered volume of up to $16.7 \times 12.5 \times 18.8$ cm, without support for occlusions.

In our setup (shown in Figure 3), we exchanged the 2D display with an integral imaging display by substituting the LCD with a rear-projected emissive screen in conjunction with a micro-lens array placed on top. Our display is therefore able to support volumetric layers with occlusion effects, in contrast to [SSR12]. A high-speed DLP projector (Light Commander from Logic PD) provides monochrome images that are synchronized to the vibration of the mirror. Using the projector's monochrome mode, we are able to achieve up to 24 images per stroke of the mirror at an aggregate frame rate of 1440 frames per second, forming up to 24 image planes at 60 Hz. The microlens array is comprised of staggered 2D fly's eye lenslets in a close-packed hexagonal format, in order to support both horizontal and vertical ray separation of the underlying image. The Light Commander's image size (at a resolution of 1024x768 pixels) is chosen to provide 13 pixels horizontally and 11.3 pixels vertically under each lenslet. The field of view of the lenslets (41°) exceeds the field of view of the volumetric display (19°). We therefore pad the outer viewing rays to reduce light transmission through the seams between the individual lenses, which

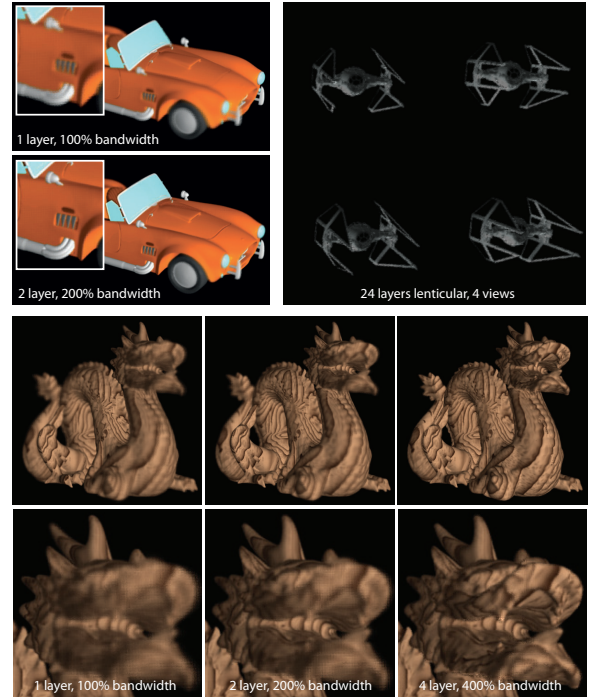


Figure 4: Simulated display results. The overall depth of field increases when using multiple layers, supporting large parallax movement.

leads to effects similar to cross-talk. A total number of 6x6 rays are used per lenslet.

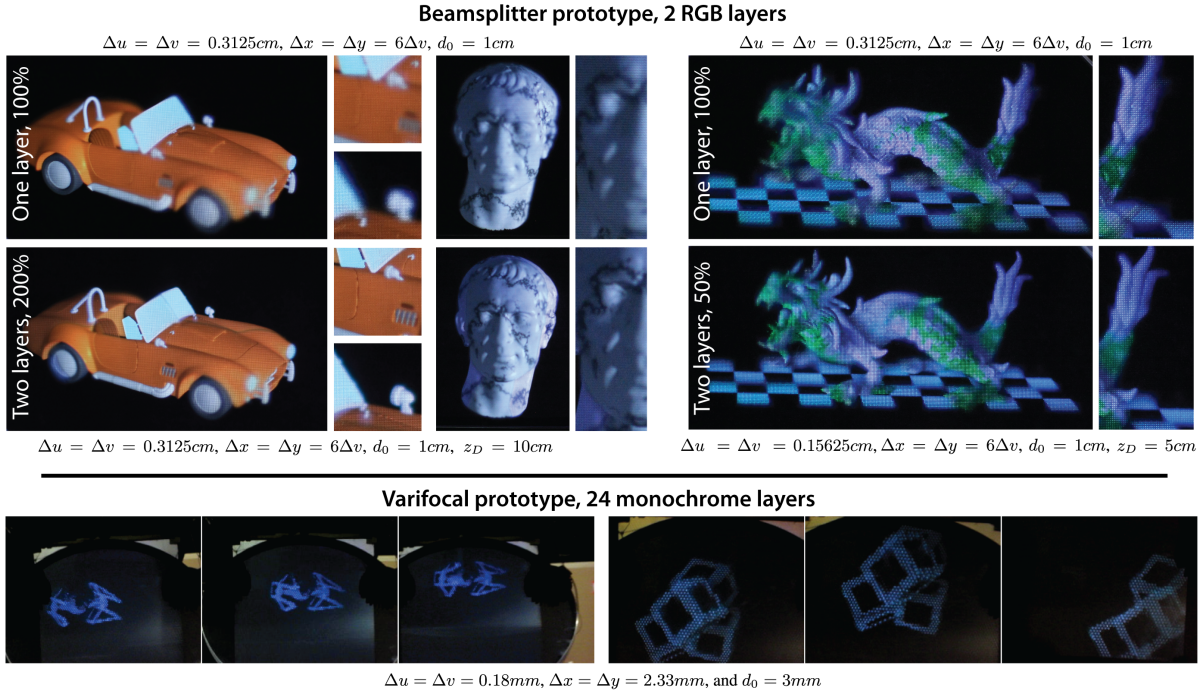


Figure 5: Results from our prototypes. The top part shows results from the dual layer beamsplitter. The car and the bust model are shown on single layer configuration with 100% bandwidth (top row), and on a dual-layer configuration with 200% bandwidth (bottom row). The dragon model is shown on a single layer configuration with 100% bandwidth (top row), and a dual layer configuration with 50% bandwidth (bottom row). Note the increased sharpness around edges and high-frequency textures. We employ 9 time-multiplexing steps to increase the spatial resolution. Photos of the dual-layer prototype are taken with a Canon Eos 1D Mark III, ISO 3200 and $\frac{1}{4}\text{s}$ exposure time. The bottom part shows results from the varifocal display. Using 24 layers, we can achieve a very wide depth of field of approximately 19 cm at wide viewing angles. Note that the layer spacing exceeds the depth resolution of human eyes, and our system therefore provides much better accommodation cues than single layer displays. Photos of the varifocal results are taken with a small hand-held PowerShot camera.

7. Results and Discussion

We evaluate the effectiveness of our approach using simulated results and results from both prototypes. The simulation results (Figure 4) show the effect of adding additional layers. With every additional layer, the depth of field increases leading to much sharper images for the outer depth ranges. In our simulation, we employed 36 time-multiplexing steps to show the results in full spatial resolution. Note, although a high number of multiplexing steps is extremely difficult to achieve with current display technology, we intend to demonstrate the effect of the increased depth of field without distracting resolution artifacts.

Figure 5 shows results captured with our beam-splitter prototype. Although using only two layers, the depth of field is already noticeably enhanced when using more bandwidth than a single layer display. The results also show that the same depth of field of a single layer display can be reproduced by two displays using only half of the overall ray count.

The results of the varifocal display prototype are shown in Figure 5. The possible depth of field (18.8cm) at wide viewing angles of 18° is huge compared to existing displays. Furthermore, by using up to 24 layers, the layer spacing exceeds the limits of human depth resolution, see [AWGB04] for more details. Therefore, our varifocal display prototype can provide nearly correct accommodation cues for content close to the display volume. Although the prototype is able to support monochrome images only, the resulting parallax movement is visible in the accompanying video.

Our display model shares the same trade-off between spatial and angular resolution as all automultiscopic displays. When increasing the number of layers, the effective angular resolution can be reduced up to one angular sample for diffuse scenes. In order to support view-dependent effects (such as glossy materials) and our occlusion approximation, however, more angular samples are needed.

For a next prototype version, we plan to use smaller lenses with higher image resolutions. While using a parallax barrier

approach reduces the brightness considerably, using lenticular arrays avoids this brightness loss at the cost of increased crosstalk. In addition, both prototypes employ optical stacking of multiple primitives which leads to a brightness reduction of $\frac{1}{n}$ for each individual layer, compared to using one layer only. Due to the stacking of multiple layers, our displays inherently do not support view repetitions that are commonly found in parallax barrier or integral imaging displays.

The varifocal mirror prototype only supports monochrome images and we hope to extend the system to a gray scale version using, for example, temporal super-sampling. Combining multiple pixels into one luminance value could be another option, by using higher resolution projectors in conjunction with diffusers that support respective blur kernels. High speed color images might become possible in the future, for example by combining multiple DLP chips into one optical system.

In our prototypes, the individual layers cannot block incoming light from other layers and therefore occlusions cannot be handled correctly. Using the implicit occlusion handling of our light field distribution algorithm, the resulting filtered object shadows will be blurred out. This can lead to noticeable black halos/shadows around the occluder, which becomes more pronounced for stronger parallax (i.e. for larger layer spacings). In our experiments, however, the shadow is barely noticeable due to the anti-alias filtering of the occluded regions. The varifocal mirror system only supports monochrome images, and unfortunately no such filtering strategies can be applied unless multiple luminance values would be supported.

Both display prototypes exhibit a substantial amount of cross-talk, which results in additional blur. The customized LCD layers furthermore exhibit a slight color difference, and low contrast, which is most likely due to imprecise the alignment of the emissive and modulating planes, as well as some slight shifts between the respective polarizers. Furthermore, alignment of the individual layers is performed manually at the moment, and some object seams are visible due to the imperfect alignment. Using calibration techniques, this issue could be mitigated.

8. Conclusion

In this paper, we introduced a hybrid display model that combines the advantages of volumetric and parallax-based displays. These multi-layered automultiscopic displays are able to show a wide depth of field for horizontal and vertical parallax, large viewing angles, and better accommodation cues that have been difficult to achieve by other displays. We presented a corresponding bandwidth analysis, and showed that multiple layers can reproduce the same content for diffuse scenes using a smaller ray count compared to a single layer. A simple and efficient algorithm can be

used to distribute an input light field onto multiple layers, and we demonstrated a light-weight extension to existing ray tracing frameworks in order to support synthetic scenes. We evaluated the effectiveness of our display model using simulations and two physical hardware prototypes. The prototypes show promising results, which we hope to improve as display technology advances. In addition to extensions listed in the previous section, our work could possibly be extended by employing content-adaptive barrier techniques such as [LHKR10] or by shiftable lenslet techniques such as [JJ02]. In its current formulation, the light-field distribution algorithm requires known scene depth, but general input light fields could be supported by solving a constrained linear system, similar to [WLHR11, LWH*11].

References

- [AWGB04] AKELEY K., WATT S. J., GIRSHICK A. R., BANKS M. S.: A stereo display prototype with multiple focal distances. *ACM Transactions on Graphics* 23, 3 (2004), 804–813. [2](#) [7](#)
- [BCP*08] BELL G. P., CRAIG R., PAXTON R., WONG G., GALBRAITH D.: Beyond flat panels: Multi-layered displays with real depth. In *SID Symposium Digest of Technical Papers*, 39, 1 (2008), pp. 352–355. [2](#)
- [Ber99] BERKEL C. V.: Image preparation for 3D-LCD. *SPIE Stereoscopic Displays and Virtual Reality Systems* 3639 (1999), 84–91. [2](#)
- [Buz85] BUZAK T. S.: A field-sequential discrete-depth-plane three-dimensional display. *SID Symposium Digest* (1985), 345–347. [2](#)
- [CNH*07] COSSAIRT O. S., NAPOLI J., HILL S. L., DORVAL R. K., FAVALORA G. E.: Occlusion-capable multiview volumetric three-dimensional display. *Applied Optics* 46 (2007), 1244–1250. [2](#)
- [CTCS00] CHAI J.-X., TONG X., CHAN S.-C., SHUM H.-Y.: Plenoptic sampling. In *Proc. SIGGRAPH* (2000), pp. 307–318. [3](#)
- [Fav05] FAVALORA G.: Volumetric 3d displays and application infrastructure. *IEEE Computer* 38, 8 (2005), 37–44. [2](#)
- [FRSL08] FUCHS M., RASKAR R., SEIDEL H.-P., LENSCHE H. P. A.: Towards passive 6D reflectance field displays. *ACM Transactions on Graphics* 27, 3 (2008). [2](#)
- [GF98] GOLD R., FREEMAN J.: Layered display system and method for volumetric presentation. U.S. patent 5,813,742, 1998. [2](#)
- [Got10] GOTODA H.: A multilayer liquid crystal display for autostereoscopic 3D viewing. In *SPIE Stereoscopic Displays and Virtual Reality Systems* 7524 (2010). [2](#)
- [HBLM11] HOLROYD M., BARAN I., LAWRENCE J., MATUSIK W.: Computing and fabricating multilayer models. *ACM Transactions on Graphics* 30, 6 (2011), 187:1–187:8. [2](#)
- [Ive03] IVES F.: Parallax stereogram and process for making same. U.S. Patent No. 725,567, 1903. [1](#)
- [IYS93] ISONO H., YASUDA M., SASAZAWA H.: Autostereoscopic 3-D display using LCD-generated parallax barrier. *Electronics and Communications in Japan (Part II: Electronics)* 76, 7 (1993), 77–84. [1](#)

- [JJ02] JANG J.-S., JAVIDI B.: Improved viewing resolution of three-dimensional integral imaging by use of non-stationary micro-optics. *Optics Letters* 27, 5 (2002), 324–326. URL: <http://www.ncbi.nlm.nih.gov/pubmed/18007791>. 2, 8
- [JMW*03] JACOBS A., MATHER J., WINLOW R., MONTGOMERY D., JONES G., WILLIS M., TILLIN M., HILL L., KHAZOOVA M., STEVENSON H., BOURHILL G.: 2D/3D switchable displays. *Sharp Technical Journal*, 4 (2003), 15–18. 1
- [JMY*07] JONES A., McDOWALL I., YAMADA H., BOLAS M., DEBEVEC P.: Rendering for an interactive 360 light field display. *ACM Transactions on Graphics* 26, 3 (2007), 40:1–40:10. 2
- [KHL10] KIM Y., HONG K., LEE B.: Recent researches based on integral imaging display method. *3D Research* 1 (2010), 17–27. URL: [http://dx.doi.org/10.1007/3DRes.01\(2010\)2.2](http://dx.doi.org/10.1007/3DRes.01(2010)2.2)
- [KHY*09] KAO Y.-Y., HUANG Y.-P., YANG K.-X., CHAO P. C.-P., TSAI C.-C., MO C.-N.: An auto-stereoscopic 3D display using tunable liquid crystal lens array that mimics effects of grin lenticular lens array. *SID Symposium Digest of Technical Papers* 40 (2009), 111–114. 2
- [KKK*07] KIM Y., KIM J., KANG J.-M., JUNG J.-H., CHOI H., LEE B.: Point light source integral imaging with improved resolution and viewing angle by the use of electrically movable pinhole array. *Optics Express* 15, 26 (2007), 18253–18267. 1, 5
- [LD10] LEVIN A., DURAND F.: Linear view synthesis using a dimensionality gap light field prior. In *CVPR* (2010), pp. 1831–1838. 3
- [LHKR10] LANMAN D., HIRSCH M., KIM Y., RASKAR R.: Content-adaptive parallax barriers: optimizing dual-layer 3D displays using low-rank light field factorization. *ACM Transactions on Graphics* 29, 6 (2010), 163:1–163:10. 2, 5, 8
- [LIE98] LEUNG M. S., IVES N. A., ENG G.: Three-dimensional real-image volumetric display system and method. U.S. patent 5,745,197, 1998. 2
- [Lip08] LIPPmann G. M.: La photographie integrale. *Comptes-Rendus* 146 (1908), 446–451. 2
- [LWH*11] LANMAN D., WETZSTEIN G., HIRSCH M., HEIDRICH W., RASKAR R.: Polarization fields: dynamic light field display using multi-layer LCDs. *ACM Transactions on Graphics* 30, 6 (2011). 2, 8
- [PBD*10] PARKER S. G., BIGLER J., DIETRICH A., FRIEDRICH H., HOBEROCK J., LUEBKE D., MCALLISTER D., MCGUIRE M., MORLEY K., ROBISON A., STICH M.: Optix: A general purpose ray tracing engine. *ACM Transactions on Graphics* 29 (2010), 66:1–66:13. 5
- [PKS*08] PETERKA T., KOOIMA R. L., SANDIN D. J., JOHNSON A., LEIGH J., DEFANTI T. A.: Advances in the dynalax solid-state dynamic parallax barrier autostereoscopic visualization display system. *IEEE Transactions on Visualization and Computer Graphics* 14, 3 (2008), 487–499. 1
- [PPK00] PERLIN K., PAXIA S., KOLLIN J. S.: An autostereoscopic display. In *Proc. SIGGRAPH* (2000), pp. 319–326. 1
- [SSH*04] SUYAMA S., SAKUCHI HIDEAKI O., KAZUTAKE T., SAKAI U. S.: Apparent 3-D image perceived from luminance-modulated two 2-D images displayed at different depths. *Vision Research*, 44 (2004), 785–793. 2
- [SSR12] SMITHWICK Q., SMOOT L. S., REETZ D.: A volumetric display using a rim-driven varifocal beamsplitter and high-speed DLP backlit LCD. to appear at SID, 2012. 5, 6
- [STUS00] SUYAMA S., TAKADA H., UEHIRA K., SAKAI S.: A novel direct-vision 3-D display using luminance-modulated two 2-D images displayed at different depths. *SID Digest* (2000), 1208–1211. 2
- [Sul04] SULLIVAN A.: DepthCube solid-state 3D volumetric display. In *SPIE Stereoscopic Displays and Virtual Reality Systems* (2004), vol. 5291, pp. 279–284. 2
- [Tra67] TRAUB A.: Stereoscopic display using rapid varifocal mirror oscillations. *Applied Optics* 6, 6 (1967), 1505–1511. 2
- [TT82] TAMURA S., TANAKA K.: Multilayer 3-D display by multidirectional beam splitter. *Applied Optics* 21 (1982), 3659–3663. 2
- [Ueh07] UEHIRA K.: New depth-fused 3-D perception on 3-D display system using two stereoscopic displays. *Journal of Electronic Imaging* 16, 3 (2007). 2
- [WLHR11] WETZSTEIN G., LANMAN D., HEIDRICH W., RASKAR R.: Layered 3D: Tomographic image synthesis for attenuation-based light field and high dynamic range displays. *ACM Transactions on Graphics* 30, 4 (2011). 2, 8
- [WLHR12] WETZSTEIN G., LANMAN D., HIRSCH M., RASKAR R.: Tensor Displays: Compressive Light Field Synthesis using Multilayer Displays with Directional Backlighting. *ACM Transactions on Graphics* 31, 4 (2012), 1–11. 2
- [ZMDP06] ZWICKER M., MATUSIK W., DURAND F., PFISTER H.: Antialiasing for automultiscopic 3D displays. In *Eurographics Symposium on Rendering* (2006). 3